J Bioenerg Biomembr (2007) 39:175–185
DOI 10.1007/s10863-007-9075-0

ORIGINAL PAPER

Interaction of cationic *meso*-porphyrins with liposomes, mitochondria and erythrocytes

Fabio M. Engelmann · Ildemar Mayer · Dino S. Gabrielli · Henrique E. Toma · Alicia J. Kowaltowski · Koiti Araki · Mauricio S. Baptista

Received: 30 November 2006 / Accepted: 18 December 2006 / Published online: 14 April 2007

Abstract Two series of cationic porphyrins *meso*-(3*N*-methylpyridinium)phenylporphyrin (3P1, 3P2c, 3P2t, 3P3 and 3P4) and *meso*-(4*N*-methylpyridinium)phenylporphyrin (4P1, 4P2c, 4P2t, 4P3 and 4P4) were studied to obtain a comprehensive understanding of factors that influence the binding of cationic porphyrins to liposomes and mitochondria, as well as their photodynamic efficiencies in erythrocytes. Binding and photodynamic efficiency were found to be inversely proportional to the number of positively charged groups and directly proportional to *n*-octanol/water partition coefficients (log P_{OW}), except for the *cis* molecules 3P2c and 4P2c. In the *cis* molecules, binding and photodynamic efficiency were much higher than expected, indicating that specific interactions not accounted by log P_{OW} enhance photodynamic efficiency. The effect of mitochondrial transmembrane electrochemical potentials on cationic porphyrin binding constants was estimated to be as large as 15%, and may be useful to selectively target this organelle when promoting photodynamic therapy to induce apoptosis.

Keywords Cationic porphyrins · Amphiphilic porphyrins · Membrane binding · Partition coefficient · Erythrocyte lysis · Photodynamic activity

F. M. Engelmann · I. Mayer · D. S. Gabrielli · H. E. Toma · A. J. Kowaltowski · K. Araki · M. S. Baptista
Instituto de Química,
Universidade de São Paulo,
C. Postal 26077, CEP 05513-970,
São Paulo, Brazil

K. Araki (✉) · M. S. Baptista (✉)
Departamento de Bioquímica,
Instituto de Química-USP, PO Box 26077, 05513-970, São Paulo, SP, Brazil
e-mail: {koiaraki}@iq.usp.br
e-mail: {baptista}@iq.usp.br

Introduction

Membranes exert fundamental roles in living organisms, not only organizing tissues, cells and organelles but also influencing the concentration, diffusion, reactivity and conformation of biomolecules. Consequently, recognition, binding and permeation of molecules through specific membranes are fundamental research topics in Pharmacology. This is also valid in the area of photodynamic therapy (PDT), where the selective accumulation of a sensitizer in a specific, fast growing, tissue or pathogenic microorganism is of prime importance (Lawrence et al., 1995; Dougherty et al., 1998; Zeitouni et al., 2003; Reddi et al., 2002; Smijs and Schuitmaker, 2003; Lambrechts et al., 2004; Lambrechts et al., 2005; Kramer-Marek et al., 2006; Silva, 2005; Spesia et al., 2005; Ricchelli et al., 2005). After photosensitizer accumulation, irradiation with red or near infrared light (photodynamic window) in the presence of molecular oxygen generates reactive species that cause cell damage and death. Cellular membranes and organelles are considered the main targets of photodynamic action (Villanueva and Jori, 1993; Ben Amor and Jori, 2000; Dougherty et al., 1998) and may also control the mechanisms of photodynamic action (Junqueira et al., 2002; Severino et al., 2003). However, it is important to mention that the poor binding of photosensitizes to cellular membranes is not always a disadvantage. For example, in blood infections, it is important for the photosensitizer not to bind to cell membranes with large affinity, in order to specifically target the pathogenic microorganism proteins, preserving blood cells (Casteel et al., 2004).

Many studies on the interaction of porphyrin derivatives with cells or organisms are described in the literature (Spesia et al., 2005; Villanueva and Jori, 1993; Ben Amor and Jori, 2000). This body of work indicates that the hydrophobic/hydrophilic balance plays an important role in this

process (Ricchelli et al., 2005). As a result, *n*-octanol/water partition coefficients (log P_{OW}) are commonly used as a parameter to predict the interaction of photosensitizers with membranes. However, there are few systematic studies correlating molecular structure, membrane binding properties and photodynamic efficiency (Lavi et al., 2002; Ben-Dror et al., 2006; Bronshtein et al. 2004; Woodburn et al., 2002; Kepczynski et al., 2002; Meng et al., 1994). Although some works show that the photosensitizer activity is a function of its log P_{OW} value, amphiphilic character has also been associated with enhanced photo-activity in cell cultures and in field studies of photo-insecticides. The molecular reasons for this enhanced activity have not been identified (Ben Amor and Jori, 2000).

The nature of the electric charge of porphyrin derivatives also seems to play an important role in the interaction with biological targets and photodynamic efficiency. Positively charged porphyrins accumulate more readily in cultured cells, suggesting a significant electrostatic contribution (Lambrechts et al., 2004; Kramer-Marek et al., 2006; Spesia et al., 2005; Ricchelli et al., 2005). Merchat and coauthors (Merchat et al., 1996) showed that cationic porphyrins inactivate Gram-negative (G^-) bacteria more efficiently than anionic ones, and that this behavior is attributable to their capacity to remain bound even after washing. Coulombic forces of cationic porphyrins by cellular membranes of G^- bacteria have been shown to be one of the main factors responsible for this interaction, which is weakened when the ionic strength of the medium is increased (Lambrechts et al., 2004). However, with few exceptions, the reasons for enhanced binding and photodynamic efficiency of a specific cationic porphyrin are not clearly known to date.

Furthermore, cellular sub-localization is affected by the lipophilicity of the photosensitizer and the nature of its electronic charge (positive or negative). The accumulation and induced photodamage of three porphyrin derivatives (two cationic and one anionic) was studied in HeLa cells and only the cationic lipophilic species accumulated and induced photodamage to mitochondria (Cernay and Zimmermann, 1996). Other studies showed that the anionic porphyrin TPPS presents high affinity for lysosomes and does not accumulate in mitochondria (Schneckenburger et al., 1995; Stromhaug et al., 1997; Strauss et al., 1995). A comprehensive study on the effect of picket fence porphyrins on the activity of mitochondrial enzymes has shown that photo-inactivation efficiency depends on chain length and the atropoisomer configuration of the o-phenyl substitutes (Barber et al., 1991). We have shown that the accumulation and photochemical properties of methylene blue, a positively charged sensitizer, is dependent on the electrochemical membrane potential of mitochondria (Gabrielli et al., 2004). Several other positively charged species were shown to bind to mitochondria, and this has become a new focus in drug development research (Ricchelli et al., 2005; Morgan and Oseroff, 2001; Kessel and Luo, 1998; Kessel and Luo 1999). In fact, the ability to promote apoptotic cell death secondary to membrane damage caused by oxidative stress makes mitochondria a particularly interesting target in PDT (Gabrielli et al., 2004; Morgan and Oseroff, 2001; Kessel and Luo, 1998; Kessel and Luo 1999).

In this work, we present a systematic study of porphyrin binding to membranes and their photo-damaging efficiency, using two series of porphyrins with positively charged *N*-methylpyridinium groups at the *meta* or *para* positions relative to the porphyrin ring. The number of such groups bound to the periphery of the porphyrin ring was varied from 1 to 4 in each series (Scheme 1) and their interaction with three different systems (lipid vesicles, isolated mitochondria and erythrocytes) was evaluated. In this manner, a comprehensive understanding of the contribution on photodynamic efficiency of several parameters, including the number of cationic groups around the porphyrin ring, *n*-octanol/water partition coefficients and membrane binding constants could be attained and experimentally verified, while keeping the singlet oxygen efficiency generation (S_Δ) constant.

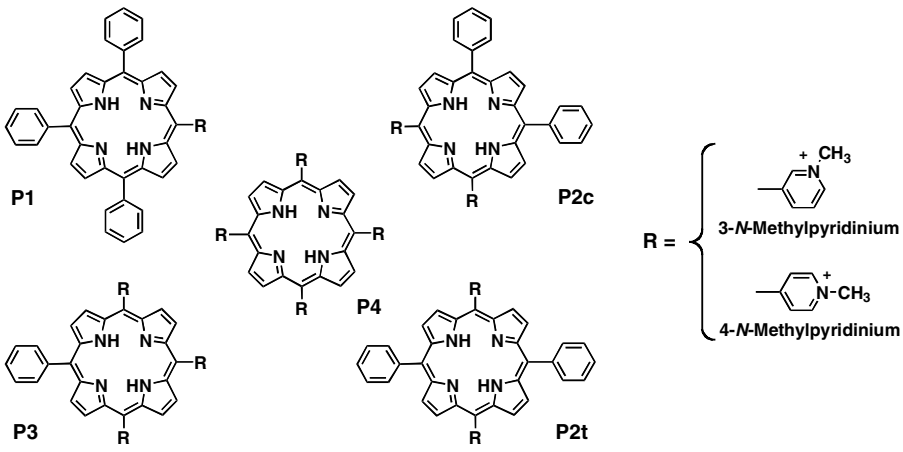

Scheme 1 Structure of *meso*-(3-*N*-methylpyridium)phenylporphyrins (series 3: 3P1, 3P2c, 3P2t, 3P3 and 3P4), and *meso*-(4-*N*-methylpyridinium)phenylporphyrins (series 4: 4P1, 4P2c, 4P2t, 4P3 and 4P4), containing 1–4 cationic groups in the periphery of the macrocyclic ring

Materials and methods

Photosensitizers

Meso-(4-*N*-pyridyl)phenylporphyrin and *meso*-(3-*N*-pyridyl) phenylporphyrin derivatives with one, two, three and four pyridyl groups were synthesized and purified as described previously (Engelmann et al., 2002) (Scheme 1). The methylated derivatives were obtained by refluxing the corresponding *meso*-phenyl(pyridyl)porphyrins with an excess of methyl tosylate in *N*,*N*′-dimethylformamide (DMF) for 4 hours. The solids were obtained by precipitation of the respective compounds as hexafluorophosphate salts by addition of an aqueous $NaPF_6$ solution. They were then dissolved in DMF and poured into a LiCl-saturated acetone solution in order to precipitate the chloride salts, which exhibit much higher solubility in water. The solids were filtered and washed several times with acetone and dried under vacuum. The series of cationic porphyrins obtained in this manner (here named series 3 and 4) are isomers and distinguished from each other by the relative position of positively charged *N*-methylpyridinium groups around the macrocyclic ring, as shown in Scheme 1. The out-of-plane disposition of the cationic groups in series 3 confers them higher polarity and water solubility. All porphyrin derivatives were soluble in water except 3P1 and 4P1, and their structures were confirmed by ^{1}H-NMR. Only the peaks related to the respective molecules and to the solvent were found in the spectra, demonstrating the purity of the porphyrin samples.

3P1

meso-mono(3-*N*-methyl-pyridyl)triphenylporphyrin chloride; ^{1}H-NMR (300 MHz, acetone$_{d6}$): δ = 10.08 (s, 1H), 9.63 (d, 1H), 9.54 (d, 1H), 8.95 (m, 8H), 8.76 (t, 1H), 8.25 (d, 6H), 7.85 (m, 9H), 4.99 (s, 3H) and −2.80 ppm (s, 2H).

3P2t

meso-di-trans(3-*N*-methyl-pyridyl)diphenylporphyrin dichloride; $\varepsilon_{417\,nm} = 2.4 \times 10^5$ in H_2O and $\varepsilon^H{}_{437\,nm} = 2.7 \times 10^5\,M^{-1}\,cm^{-1}$ in H_3O^+; ^{1}H NMR (300 MHz, DMSO$_{d6}$): δ = 9.99 (d, 2H), 9.48 (d, 2H), 9.37 (broad peak), 2H), 9.08 (d, 4H), 8.95 (d, 4H), 8.58 (t, 2H), 8.22 (d, 4H), 7.89 (m, 6H), 4.65 (s, 6H) and −3.00 ppm (s, 2H).

3P2c

meso-di-cis(3-N-methyl-pyridyl)diphenylporphyrin dichloride; $\varepsilon_{417\,nm} = 2.0 \times 10^5$ in H_2O and $\varepsilon^H{}_{437\,nm} = 2.4 \times 10^5\,M^{-1}\,cm^{-1}$ in H_3O^+; ^{1}H NMR(300 MHz, acetone$_{d6}$): δ = 10.07 (s, 2H), 9.59 (d, 2H), 9.50 (d, 2H), 9.05 (m, 8H), 8.73 (t, 2H), 8.26 (d, 4H), 7.87 (m, 6H), 4.96 (s, 6H) and −2.84 ppm (s, 2H).

3P3

meso-tri(3-*N*-methyl-pyridyl)monophenylporphyrin trichloride; $\varepsilon_{417\,nm} = 2.4 \times 10^5$ in H_2O and $\varepsilon^H{}_{437\,nm} = 2.5 \times 10^5\,M^{-1}\,cm^{-1}$ in H_3O^+; ^{1}H NMR (300 MHz, acetone$_{d6}$): δ = 10.09 (s, 3H), 9.60 (m, 3H), 9.51 (m, 3H), 9.14 (m, 8H), 8.74 (m, 3H), 8.26 (d, 2H), 7.90 (m, 3H), 4.96 (s, 6H), 4.94 (s, 3H) and −2.90 ppm (s, 2H).

3P4

meso-tetra(3-*N*-methyl-pyridyl)porphyrin tetrachloride; $\varepsilon_{417\,nm} = 2.6 \times 10^5$ in H_2O and $\varepsilon^H{}_{437\,nm} = 3.0 \times 10^5\,M^{-1}\,cm^{-1}$ in H_3O^+; ^{1}H NMR (300 MHz, acetone$_{d6}$): δ = 10.07 (s, 4H); 9.61 (d, 4H); 9.49 (d, 4H); 9.24 (s, 8H), 8.73 (t, 4H), 4.93 (s, 12H) and −2.99 ppm (s, 2 H).

4P1

meso-mono(4-*N*-methyl-pyridyl)triphenylporphyrin- chloride; ^{1}H NMR (300 MHz, DMSO$_{d6}$): δ = 9.33 (d, 2H), 8.91 (m, 10H), 8.18 (d, 6H), 7.83 (m, 9H), 4.66 (s, 3H) and −2.97 ppm (s, 2H).

4P2t

meso-di-trans(4-N-methyl-pyridyl)diphenylporphyrin dichloride; $\varepsilon_{425\,nm} = 1.8 \times 10^5$ in H_2O and $\varepsilon^H{}_{455\,nm} = 2.0 \times 10^5\,M^{-1}\,cm^{-1}$ in H_3O^+; ^{1}H NMR (300 MHz, DMSO$_{d6}$): δ = 9.47 (d, 4H), 9.01 (d, 8H), 8.96 (d, 4H), 8.23 (d, 4H), 7.88 (m, 6H), 4.69 (s, 6H) and −2.98 ppm (s, 2H).

4P2c

meso-di-cis(4-*N*-methyl-pyridyl)diphenylporphyrin dichloride; $\varepsilon_{425\,nm} = 1.1 \times 10^5$ in H_2O and $\varepsilon^H{}_{455\,nm} = 1.5 \times 10^5\,M^{-1}\,cm^{-1}$ in H_3O^+; ^{1}H NMR (300 MHz, DMSO$_{d6}$): δ = 9.43 (d, 4H), 9.01 (m, 12H), 8.23 (d, 4H), 7.86 (m, 6H), 4.69 (s, 6H) and −2.96 ppm (s, 2H).

4P3

meso-tri(4-*N*-methyl-pyridyl)monophenylporphyrin trichloride; $\varepsilon_{425\,nm} = 1.5 \times 10^5$ in H_2O and $\varepsilon^H{}_{455\,nm} = 1.7 \times 10^5\,M^{-1}\,cm^{-1}$ in H_3O^+; ^{1}H RMN (300 MHz, DMSO$_{d6}$): δ = 9,51 (d, 6H), 9,10 (m, 14H), 8,24 (d, 2H), 7,88 (m, 3H), 4,73 (s, 9H) and −3,01 ppm (s, 2H).

4P4

meso-tetra(4-*N*-methyl-pyridyl)porphyrin tetrachloride; $\varepsilon_{425\,nm} = 1.8 \times 10^5$ in H_2O and $\varepsilon^H{}_{455\,nm} = 2.3 \times 10^5\,M^{-1}\,cm^{-1}$ in H_3O^+; ^1H NMR (300 MHz, $DMSO_{d6}$): $\delta = 9.48$ (d, 8H), 9.18 (s, 8H), 8.87 (d, 8H), 4.72 (s, 12H) and −3.10 ppm (s, 2H).

Singlet oxygen generation efficiency ($\mathbf{S}_\Delta$)

$\mathbf{S}_\Delta$ values were determined from phosphorescence decay curves at 1270 nm. The data were recorded with a time-resolved NIR fluorometer (Edinburgh Analytical Instruments) equipped with a Nd:YAG laser (Continuum Surelite III) for sample excitation at 532 nm. The emitted light was passed through a silicon filter and a monochromator before detection by NIR-PMT (Hamamatsu Co. R5509) (Gabrielli et al., 2004; Severino et al., 2003). The experiments were performed at room temperature, in air-saturated D_2O solution. The sample absorbance was adjusted to 0.3 a.u. (∼0.2 mM) at 532 nm and ϕ_Δ values were calculated using equation 1:

$$S^b_\Delta = \phi^a_\Delta \frac{I^b}{I^a} \quad (1)$$

where ϕ^a_Δ and I^a are, respectively, the quantum yield (0.90, D_2O) (Redmond and Gamlin, 1999) and the phosphorescence intensity of $^1O_2$ at 1270 nm of the 4P4 species, which was used as standard. I^b is the phosphorescence emission intensity of the other cationic porphyrin derivatives.

Partition coefficient in *n*-octanol/water (log P_{OW})

n-octanol/water partition coefficients were measured using a modification of the shake-flask method as approached by Collander (Collander, 1951) and confirmed by Seiler (Seiler, 1974) and El Tayar (Eltayar, 1991). The partition data were obtained in a more convenient *n*-butanol/water system and converted to log P_{OW} using a correlation curve, as described in detail elsewhere (Engelmann et al., 2007).

Preparation of multilamellar vesicles (MLV)

MLV were chosen because they allow easy separation of the bound and free porphyrins by centrifugation. In order to mimic the lipid composition of the internal mitochondrial membrane, vesicles were prepared with 20% cardiolipin (heart-disodium salt, CL) and 80% 1,2-distearoyl-sn-glycero-3-phosphocholine (DSPC). An ethanolic solution with 6.3 mg (8 μmols) DSPC and 3.0 mg (2 μmols) CL, both from Avanti Polar Lipids®, was dried in an argon flux to form a film. 2 mL of 5 mM Tris/HCl pH = 7.2 buffer solution were added and the system was vortexed for 3 min. The suspension was centrifuged for 3 min at 15000 rpm, 25°C, and the supernatant (containing smaller vesicles) was discarded. An equivalent volume of buffer solution was added and the pellet was re-suspended. This procedure was repeated at least twice and the final lipid concentration was determined using the molybdate method (Rouser et al., 1970).

Preparation of mitochondria

Mitochondria were isolated from the livers of fasting 250–300 g adult Sprague-Dawley rats by differential centrifugation, as described previously (Gabrielli et al., 2004). The protein concentration in the final suspension was determined using the Biuret method (Netto et al., 2002), and adjusted to ∼12 mg mL^{-1}. The mitochondrial suspension was kept over ice and used within 5 hours of the preparation.

Binding constants

Direct measurements of porphyrin partition between liposomes or mitochondria and their solvent were obtained by centrifugation (the suspensions were centrifuged for 3 min at 1.3×10^4 g at 25°C) and separation of bound and free porphyrin species. Mitochondrial suspensions were incubated in media containing 250 mM sucrose, 10 mM Hepes, 1 mM EGTA, 2 mM succinate, 1 mM phosphate, pH = 7.2 (KOH), 1 μM oligomycin, and 1 μM rotenone, at 37°C. After addition of porphyrin, the sample was incubated for 3 min and centrifuged at 13000 rpm for 2 min. 0.7 mL of the supernatant was collected and acidified with 50 μL of a 22% HCl solution (v/v). The porphyrin concentration was determined spectrophotometrically at 438 nm (quartz cuvette, 0.4 cm optical pathlength). This strategy was applied to avoid the adsorption of porphyrin by the cuvette walls. The mitochondrial pellet was also dissolved with HCl to release the porphyrin, followed by absorption measurements at 446 nm. A similar procedure was used to measure binding constants with the vesicles, but the samples were incubated for one hour instead of 3 minutes. Porphyrin solutions (∼8 μM) were prepared in 5 mM Tris/HCl pH = 7.2 buffer solutions. In the mitochondrial experiments, the influence of the mitochondrial electrochemical inner membrane potential was verified by carrying out similar experiments using a proton ionophore (CCCP, carbonyl cyanide *m*-chlorophenylhidrazone, 3 μM) to eliminate the proton gradient.

The binding constants of the cationic porphyrin derivatives to MLV vesicles (K^V_B) or mitochondria (K^M_B) were estimated considering that each site is able to bind only one cationic porphyrin molecule (Eq. 2) (Angeli et al., 2000; Voszka et al., 1999) and the number of available MLV and mitochondrial binding sites were estimated by the total

number of cis-porphyrin bound to the membranes. Because the *cis*-porphyrin showed an extremely large affinity toward the membranes, we assumed that this porphyrin was able to saturate all available binding sites when present in large excess. Therefore, the values of available binding sites ([B]) were calculated by the concentration of *cis*-porphyrin bound at saturation ($[P–B]_{sat}$, see Figs. 4A and 4E). This is an important assumption since we intended to compare the binding affinities of both series of cationic porphyrin derivatives with significantly different membrane systems.

$$[P] + [B] \overset{K_B}{\rightleftharpoons} [P-B]$$
$$K_B = \frac{[P-B]}{[P][B]} = \frac{[P-B]}{[P]([P-B]_{sat} - [P-B])} \quad (2)$$

The experiments were carried out by adding increasing amounts of porphyrin to a constant MLV (0.1 mM) or mitochondrial ($0.22\,mg\,mL^{-1}$) concentration. The maximum amount of cationic porphyrin ($[P\text{-}B]_{sat}$) that is bound to the vesicle and to mitochondria is measurable. The concentrations of free ([P]) and bound ([P-B]) porphyrin molecules were determined from the UV-Vis spectra of the supernatant solution and of pellet generated after centrifugation, as described below.

Photodynamic efficiency

Erythrocytes were used to evaluate the photodynamic efficiency of cationic porphyrin sensitizers. Blood (∼3 mL) was collected by cardiac puncture of fasting, anesthetized 250–300 g adult Sprague-Dawley rats. 2 mL citrate solution (3% in PBS) and 10 mL of PBS were added. The erythrocytes were separated by centrifugation at 2000 rpm, 4°C, for 3 min. The supernatant was discarded and the pellet re-suspended in the same volume of PBS. After repeating the procedure 3 times, suspensions containing $\sim 1.3 \times 10^9$ cells mL^{-1} were obtained, as assessed by cell counts in a hemocytometer. The efficiency of cell lysis was assessed by measuring the decrease in light scattered by the erythrocyte suspension, under constant irradiation (Khalili and Grossweiner, 1997) in the absence and presence of porphyrin photosensitizers. The experiments were carried out in a quartz cuvette (1.0 cm optic path length) with constant stirring. 3 μL of the erythrocyte suspension were added to 3 mL of a 6 μM porphyrin solution and the transmission at 650 nm was measured as a function of the time. A Nd:YAG laser (20 mW, 532 nm) was employed as the light source, irradiating in an orthogonal arrangement. The lysis rates were obtained from the first derivative of the absorbance at 650 nm (due to scattering) as a function of time.

Results

Efficiency of singlet oxygen generation ($\mathbf{S}_\Delta$)

The $\mathbf{S}_\Delta$ plot of series 3 and 4 porphyrin derivatives as a function of the number of cationic *N*-methylpyridinium groups at the periphery of the porphyrin ring is shown in Fig. 1. Note that series 3 photosensitizers exhibit similar $\mathbf{S}_\Delta$ values (∼0.9), while in series 4, $\mathbf{S}_\Delta$ is proportional to the number of positively charged groups. There is no reason to assume that the decrease in $\mathbf{S}_\Delta$ in series 4 is taking place due to an intramolecular quenching effect related to the different stereochemistry of the *N*-methylpyridinium group, since similar efficiencies were obtained for the 3P4 and 4P4 species. However, aggregation is known to reduce $\mathbf{S}_\Delta$ (Junqueira et al., 2002; Severino et al., 2003; Gabrielli et al., 2004). In the *meta*-isomers, the cationic *N*-methyl groups are above and below the porphyrin ring, disfavoring association by π-stacking. The fact that the $\mathbf{S}_\Delta$ values in series 3 remain equal to 0.9 is strong evidence that there are no dimers present. In the *para*-isomers, the stereochemistry favors π-stacking, suggesting that $\mathbf{S}_\Delta$ decreases in series 4 are a consequence of aggregation, which becomes increasingly significant as the number of cationic groups decrease. It is important to mention that resonant light scattering (RLS) measurements (Kano et al., 2000; Severino et al., 2003) were performed for all porphyrin derivatives and the characteristic spectral features of large aggregates were absent in the experimental conditions used in this work, ruling out the presence of large aggregates in both series (Kano et al., 2000; Parkash et al., 1998; Dixon and Steullet, 1998; Csik et al., 1998).

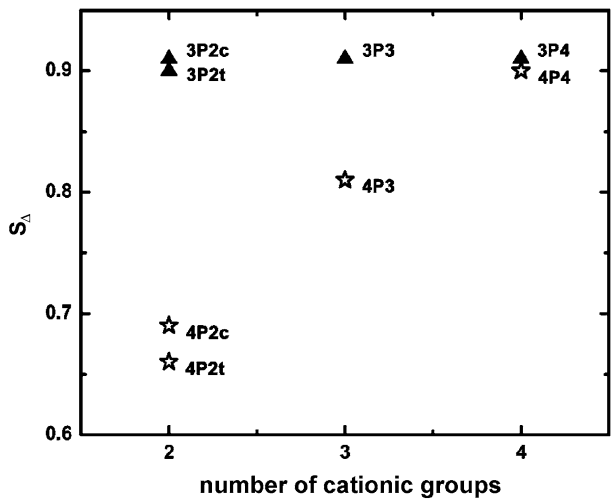

Fig. 1 Plot of singlet oxygen efficiency production (S_Δ) versus the number of cationic *N*-methylpyridinium groups in the *meta* (▲) and *para* (⋆) isomers.

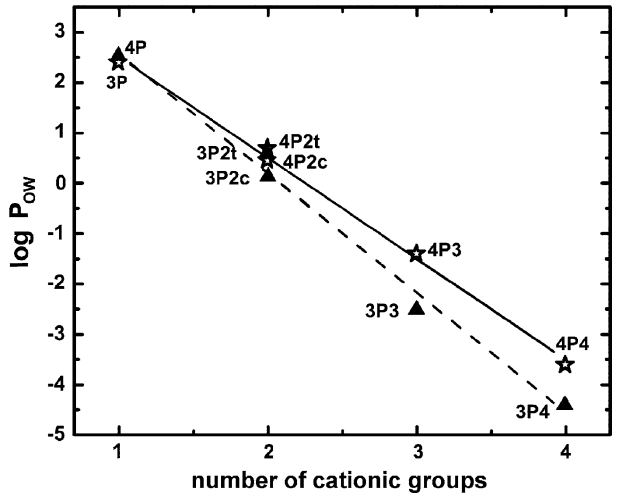

Fig. 2 Plot of the logarithm of partition coefficients in *n*-octanol/water ($\log P_{OW}$) as a function of the number of cationic groups in the photosensitizer for *meta* (▲) and *para* (⋆) isomers. Averages of 4 measurements are plotted

Partition coefficient in *n*-octanol/water ($\log P_{OW}$)

We observed that $\log P_{OW}$ increases as the number of positively charged groups decrease, following the order P4 < P3 < P2c < P2t < P1 (Fig. 2). Log P_{OW} is negative for the first two porphyrins and positive for the remaining three, showing an increasing tendency to partition into the lypophilic *n*-octanol phase. The *meta*-isomers exhibited lower $\log P_{OW}$ values than the corresponding *para*-isomers, consistent with their higher solubility in water and lower molecular symmetry. Furthermore, there is a small but significant difference between the *cis* and *trans*-isomers. The *trans*-isomers have larger $\log P_{OW}$ values than the *cis*, as expected from the symmetric disposition of the *N*-methylpyridinium groups and consequent lower dipole moments.

Vesicle binding

Other authors (Angeli et al., 2000; Voszka et al., 1999; Csik et al., 1998; Ben-Dror et al., 2006) have measured binding constants of cationic porphyrins to vesicle membranes. In all cases, measurements of binding constants were based on spectroscopic techniques in which the concentrations of free and bound species were evaluated from the changes in the absorbance or emission intensity upon binding. In the present work, the amounts of free and bound species were directly measured.

Figure 3(A–D) shows the plot of bound and free porphyrin concentrations as a function of total porphyrin concentration. The relative affinities and total amounts of the photosensitizers that can bind to the vesicles can be readily compared. A saturation pattern was observed, while the amount of bound porphyrin clearly decreases with the increase in number of charged groups in the porphyrin ring.

Determining precisely the association equilibrium constants in such a complicated system is difficult, but the data in Fig. 3A–D can be used to estimate the relative constants for the series. This was done by assuming a simple binding isotherm as depicted by Eq. 2, assuming that [B] is the total lipid concentration (available to bind porphyrins) in the low porphyrin concentration region. Because all other equilibriums that may be present, such as complex formation between lipid and porphyrin molecules (Hidalgo et al., 2005), were neglected, the equilibrium constants determined in such a way should be valid within the series for comparative purposes.

K_B^V values, which are in the $10^5\ M^{-1}$ range, are inversely proportional to the number of cationic groups and directly proportional to Log P_{OW} (Fig. 4A). Although the electrostatic interaction between the P4 species and the negatively charged membrane is larger, the doubly charged porphyrins bind much more effectively, demonstrating that hydrophobic interactions are the predominant factor defining affinity. In addition, it is evident that the *cis*-isomers 3P2c and 4P2c exhibit larger affinity than expected, considering partition coefficients. This may be accounted for by the special molecular structure of that isomer, which contains a hydrophilic head and lipophilic tail, conferring an amphiphilic character that assists the incorporation of the *cis*-isomer into the lipid membranes.

Mitochondrial binding

Mitochondria present a negative potential across their inner membrane when incubated in the presence of respiratory substrates, and constitute a system with many possible sites of interaction with cationic porphyrins (Chen, 1998). The binding titration curves obtained with mitochondria are similar to those obtained with vesicles, i.e., the total amount of bound porphyrin decreases in the order: 3P2c > 3P2t > 3 P3 >3P4 (Fig. 3, E–H). This clearly indicates that the factors influencing binding are similar in both cases. The calculated values of mitochondrial binding constants (K_B^M) increase in the order P4 < P3 < P2t < P2c, which is the same order obtained for vesicles (Table 1). The 4P2c binding constant was about 6, 11 and 20 times larger than for 4P2t, 4P3, and 4P4, respectively. The plot of K_B^M as a function of log P_{OW} (Fig. 4B) also shows a similar trend compared to the results obtained for vesicles. Therefore, a linear variation was observed for all porphyrins except for the *cis*-isomers, which exhibit much larger binding constants than those predicted based only on log P_{OW} values.

Another aspect that may influence binding of porphyrins to mitochondria is the electrostatic attraction between the negative matrix and positively charged porphyrins. To test

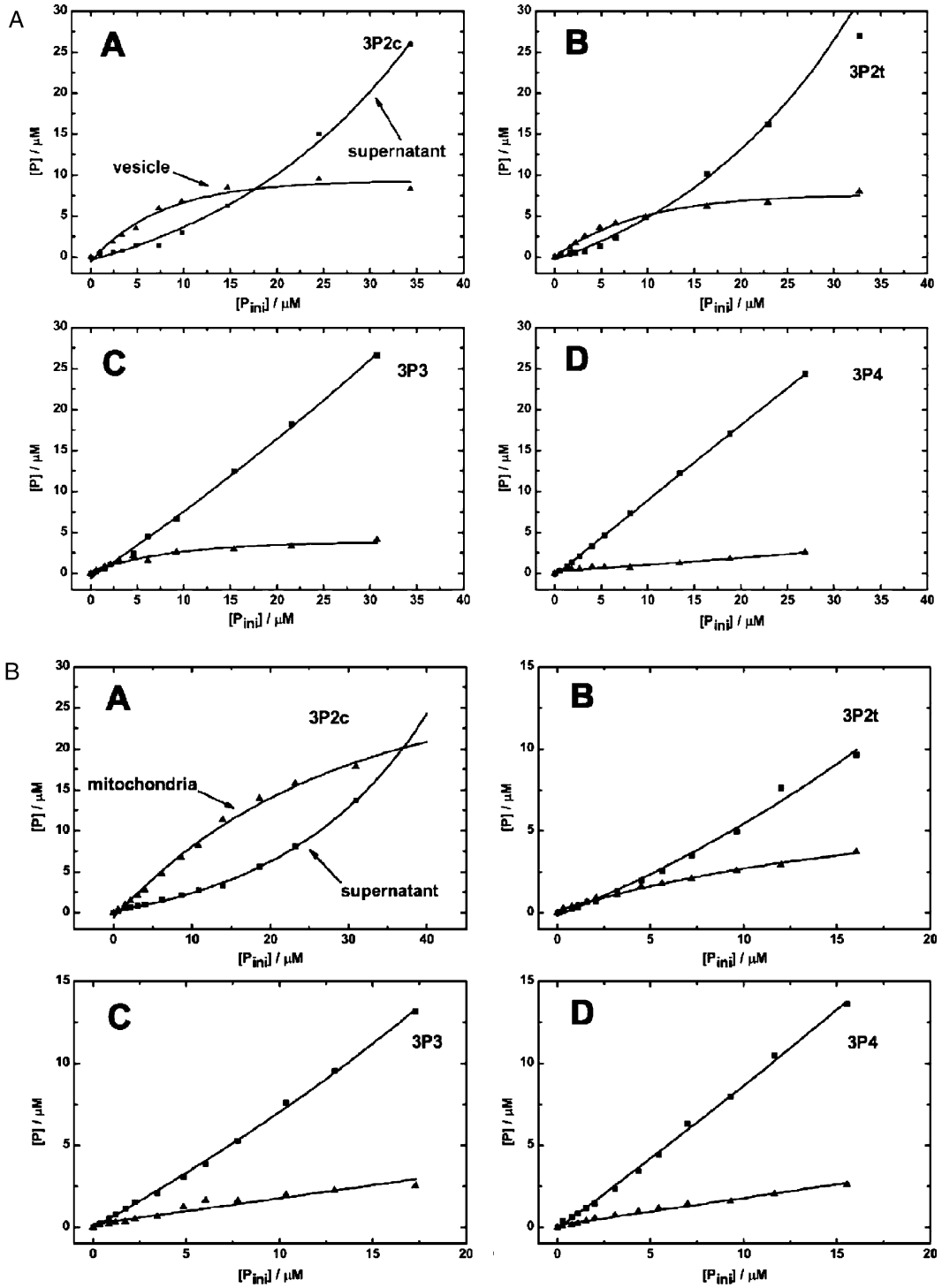

Fig. 3 Plot of free (■) and bound (▲) cationic porphyrins (3P2c, 3P2t, 3P3 and 3P4) as a function of the amount of porphyrin ($[P_{ini}]$) added to liposomes (A, [L] = 0.1 mM) or mitochondria (B, E-H, [M] = 0.22 mg mL^{-1})

the effect of the mitochondrial inner membrane potential, binding efficiencies were determined in the presence and absence of CCCP, a proton ionophore that eliminates the proton gradient (Gabrielli et al., 2004).

When CCCP was added, binding constants decreased 15.0, 14.5, 8.2 and 7.4% for 3P2c and 3P2t, and 3P3 and 3P4 species, respectively. These results indicate that the electrostatic potential exerts a significant contribution toward binding affinity. Notice that the effect was smaller for the tetracationic and tricationic 3P4 and 3P3 species relative to bicationic 3P2c and 3P2t. Evidently, the effect of electrostatic attraction is not defined exclusively by the number

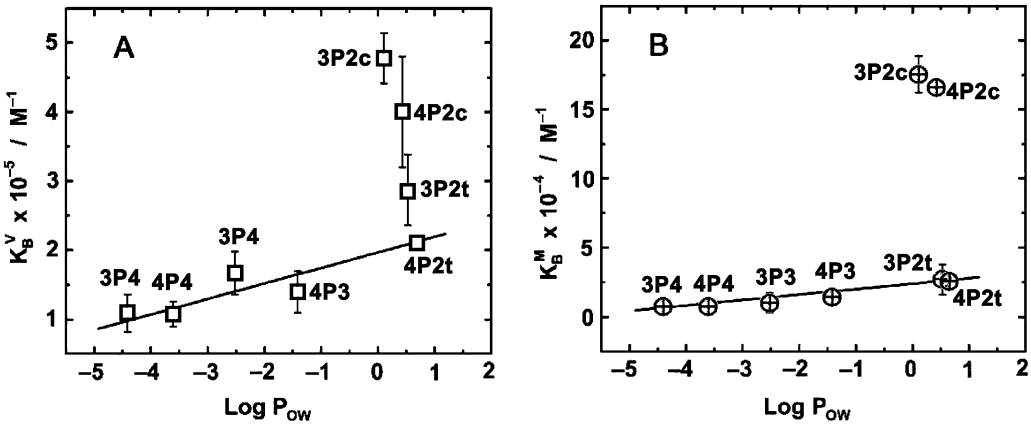

Fig. 4 Plots of the *meta*-series cationic porphyrin derivative binding constants as a function of log P_{OW} to vesicles (A) and mitochondria (B). Results represent averages ± standard deviations of 4 repetitions (or experiments)

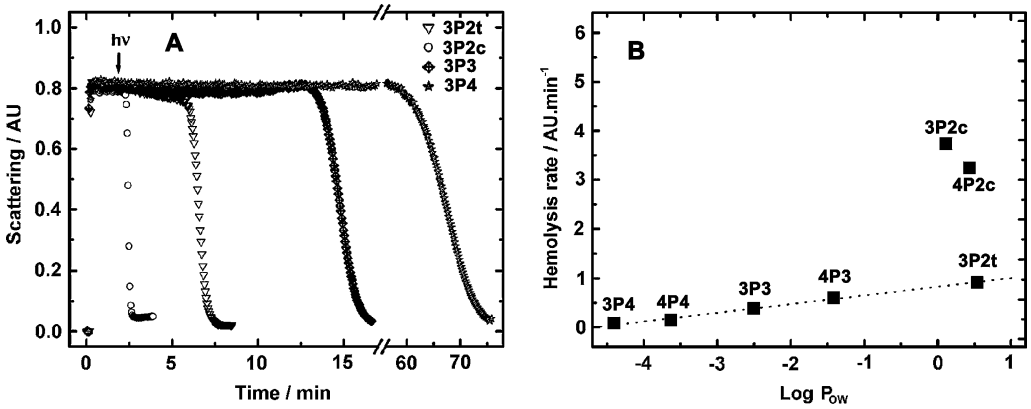

Fig. 5 (A) Photodamage induced by series 3 cationic porphyrins on erythrocytes monitored at 650 nm as a function of time. The diode laser (532 nm, 20 mW/cm^2) was turned on 0.6 min after the addition of 4 μL of an erythrocyte suspension (0.7 a.u.) to 1 mL of a cationic porphyrin in PBS (indicated by an arrow). (B) Linear correlation between hemolysis rate and log P_{OW}. The results shown are representative of a series of 4 similar repetitions

of positive charges, but rather involves other contributions. Among them, the localization of the photosensitizer in the membrane is probably a key factor (Lavi et al., 2002; Ben-Dror et al., 2006). In the case of mitochondrial binding, it seems that species that can penetrate within the membrane, approaching the negatively charged matrix, are more strongly stabilized by electrostatic effects (Gabrielli et al., 2004).

Photodynamic efficiency in erythrocytes

The photodynamic efficiency of the series 3 and 4 porphyrins was tested using erythrocytes. Cell lysis decreases light scattering of suspensions of these cells (Fig. 5A). Note that there is an induction period in which the scattering remains almost constant, followed by a decrease in scattering. The induction time increases in the order P2c < P2t < P3 < P4 varying from 1 min for 3P2c to 65 min for 3P4. In addition to a shorter induction period, 3P2c presents a larger lysis rate, i.e., a faster decrease in scattering. The relative rate constants were estimated to be 3.73, 0.86, 0.38 and 0.06 min^{-1} for 3P2c, 3P2t, 3P3 and 3P4 (Fig. 5B), respectively. Both the induction period and lysis rate constants followed the same order as the binding constant in vesicles and mitochondria. In fact, the plot of $k_{\text{hemolysis}}$ *vs* Log P_{OW} exhibited a linear correlation (except for the *cis*-isomers) similar to that found in the K_B *vs* Log P_{OW} plot, showing a direct correlation between partition coefficients, binding constants and photodynamic efficiency. Similar results were obtained for series 4 cationic porphyrins (Fig. 5B).

The amount of porphyrins bound to erythrocytes was calculated to be ~50% (3P2c), ~25% (3P2t), ~10% (3P3) and ~10% (3P4) of the concentrations used in the photolysis experiment. Although 5 times more 3P2c is bound to erythrocytes than 3P4, based on the induction periods, lysis was estimated to be about 60 times faster for 3P2c.

Discussion

The effect of the number of charged groups as well as their disposition around the porphyrin ring on parameters that af-

fect PDT have been studied before. Whitten and co-authors have shown that inactivation of mitochondrial enzymes by picket fence porphyrins is more efficient for the asymmetric analogs, in all substituted chain-lengths. The asymmetric analogs were also shown to present larger binding to mitochondria (Barber et al., 1991). Jori and coworkers showed that photodynamic efficiency, as measured by the ability to destroy tumor and bacterial cells (Merchat et al., 1996) and fruit flies (Ben Amor and Jori, 2000) increases as the polarity decreases, reaching a maximum for amphiphilic porphyrins. These authors mention that this effect must be related to the membrane binding ability of this porphyrin. However, no experimental evidence in this direction was presented. Also, the binding and photodynamic efficiency of *meso*-substituted positively charged porphyrins were shown to be dependent on electrostatic interactions. Kepczynski and coworkers have shown that the binding of porphyrins to liposomes is correlated with their partition coefficients if porphyrins of similar structure are considered (Kepczynski et al., 2002), as confirmed in the present work. Lavi et al. showed that the penetration depth of negatively charged porphyrins in a membrane affects their photodynamic efficiency (Lavi et al., 2002). Therefore, although several factors that are important in the photodynamic efficiency of porphyrins have already been described before, they have not been consistently evaluated and correlated.

In this work we performed a comprehensive study showing the effect of the molecular structure (number and position of positively charged groups) on partition coefficients (log P_{OW}), binding constants to liposomes and mitochondria (Table 1) and photodynamic efficiency in erythrocytes. Our results clearly show that the binding either to lipid vesicles or to mitochondria is inversely proportional to polarity, which can be satisfactorily predicted by the log P_{OW} values of the porphyrins. However, this relationship is not followed by amphiphilic porphyrins, that bind to vesicles or mitochondria in larger amounts and with higher affinity than would be predicted based only on log P_{OW} values. This becomes evident when the doubly charged *cis* and *trans*-isomers are compared. The first species, which is amphiphilic, presented a much larger K_B than predicted by log P_{OW}. This suggests that it has a more suitable structure to penetrate deeply into lipid membranes, maximizing hydrophobic and hydrophilic interactions, while other molecules in the series bind the membrane more superficially. A similar trend was observed by Lavi and coworkers using negatively-charged porphyrins with different size alkyl groups (Lavi et al., 2002). The special localization of the *cis*-isomers brings further free energy stabilization, not well accounted from the log P_{OW} values (Scheme 2).

Binding of porphyrins to mitochondria followed a very similar pattern. In addition, the transmembrane electrochemical potential played a significant role, particularly for species that exhibited stronger interactions, probably because they can approach the negatively charged matrix more closely. This effect has been observed for other sensitizers and uncovers the potential of positively charged sensitizers to target mitochondria preferentially (Gabrielli et al., 2004).

Another interesting aspect is the induction period observed for lysis of the erythrocytes after beginning irradiation of the suspensions with 532 nm light. Membrane lysis should happen when the amount of photogenerated reactive oxygen species (in this case mostly singlet oxygen) overcomes the antioxidant capability of the erythrocyte membrane. When the antioxidants are consumed, the membrane rapidly looses integrity. Considering that singlet oxygen generation efficiencies of the sensitizers are similar, the differences in interaction with the membranes should be the key factor to define photodynamic efficiency. However, as mentioned in the results, while binding increases by a factor of five, photodynamic effect increases by a factor of 60 within this series. Therefore, the larger differences observed in photodynamic efficiency cannot be ascribed solely to differences in the amount of porphyrin bound but must also be related to their relative position in the erythrocyte cells.

The ability of singlet oxygen to promote hemolysis has been demonstrated in several experiments. Lysis of

Table 1 Series 3 and 4 porphyrins singlet oxygen production efficiency ($S_\Delta \pm 0.05$) in D_2O, *n*-octanol/water partition coefficients (log P_{OW}), mitochondrial (K_B^M) and vesicle binding constants (K_B^V) (DSPC/CL 8:2)

	ϕ_Δ (D_2O)	logP_{OW}	$K_B^M \times 10^{-4}$ (M^{-1})	$K_B^V \times 10^{-5}$ (M^{-1})
3P	–	2.49 ± 0.00	–	–
3P2c	0.91	0.11 ± 0.08	17.5 ± 1.3	4.8 ± 0.3
3P2t	0.86	0.53 ± 0.09	2.7 ± 1.1	2.9 ± 0.5
3P3	0.91	-2.52 ± 0.09	1.0 ± 0.7	1.7 ± 0.3
3P4	0.89	-4.41 ± 0.05	1.7 ± 0.4	1.1 ± 0.3
4P	–	2.38 ± 0.09	–	–
4P2c	0.64	0.43 ± 0.08	16.6	4.0 ± 0.8
4P2t	0.61	0.68 ± 0.05	2.5	2.1 ± 0.1
4P3	0.72	-1.41 ± 0.09	1.5	1.4 ± 0.3
4P4	0.90	-3.61 ± 0.09	0.8	1.1 ± 0.2

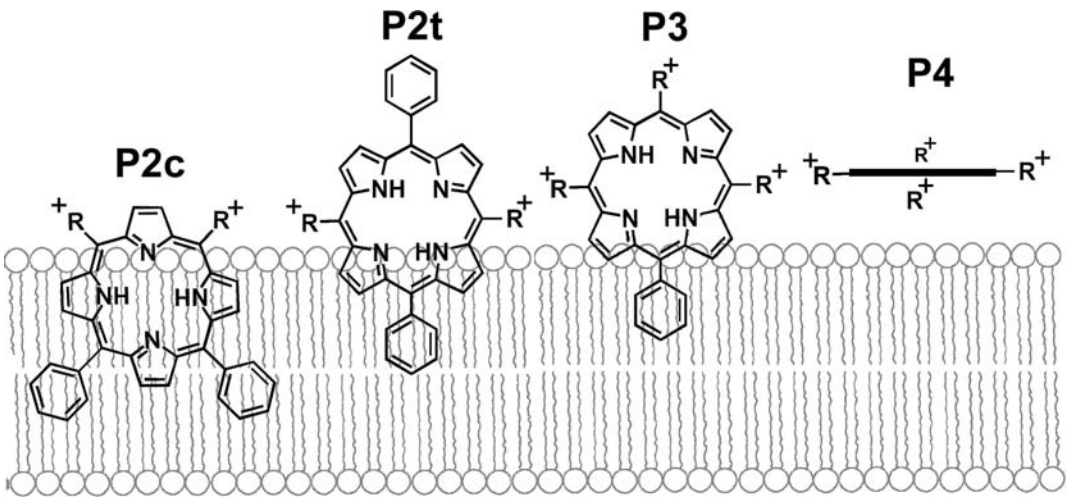

Scheme 2 Scheme showing the probable disposition of the cationic porphyrin molecules in biological membranes

biological membranes has been related to lipid oxidation and protein damage (Lissi et al., 1993). The concentration of dissolved oxygen in membranes is 2–4 times higher than in the aqueous phase and the lifetime of singlet oxygen in biological membranes is relatively low (Henderson and Dougherty, 1992; Ehrenberg et al., 1998). If the porphyrin is anchored within the membrane, the excited triplet species formed after light excitation will encounter a larger concentration of oxygen and the generated singlet oxygen will probably react with membrane components. If the sensitizer is weakly bound to the membrane interface, it will interact with lower oxygen concentrations and a larger fraction of the generated singlet oxygen will be deactivated before interacting with and oxidizing membrane components. Therefore, the higher than predicted by log P_{OW} photoactivity of the *cis*-porphyrins could be related with the fact that they can burry more deeply within the membrane, as a consequence of a more favorable molecular structure (Scheme 2).

Conclusion

The binding efficiency of cationic porphyrin sensitizers to membranes depends primarily on non-specific interactions that can be evaluated by their partition coefficients, more specifically by log P_{OW}. However, molecular structure plays a key role when the distribution of the hydrophilic and hydrophobic groups in the molecule is optimized in order to generate an amphiphilic species. The contribution of such a structural effect cannot be properly measured by log P_{OW}, indicating more specific interactions with membranes. This is probably associated with an optimized structural match that allows their incorporation within the membrane, enhancing photodynamic efficiency. There is also a significant role of the transmembrane electrostatic field that can contribute with up to 15% increases in binding constants.

Acknowledgment The financial support by *Fundação de Amparo à Pesquisa do Estado de São Paulo* (FAPESP) and *Conselho Nacional de Desenvolvimento Científico e Tecnológico* (CNPq) are gratefully acknowledged. FME is a doctoral fellow of FAPESP. We thank Edson Alves Gomes for technical support.

References

Angeli NG, Lagorio MG, SanRomán EA, et al (2000) Photochem Photobiol 72:49–56
Barber DC, VanDerMeid KR, Gibson SL, et al (1991) Cancer Res 51:1836–1845
Ben Amor T, Jori G (2000) Photochem Photobiol 71:124–128
Ben-Dror S, Bronshtein I, Wiehe A, et al (2006) Photochem Photobiol 82:695–701
Bronshtein I, Afri M, Weitman H (2004) Biophys J 87:1155–1164
Casteel MJ, Jayaraj K, Gold A, et al (2004) Photochem Photobiol 80:294–300
Cernay T, Zimmermann HW (1996) J Photochem Photobiol B: Biol 34:191–196
Chen LB (1988) Annu Rev Cell Biol 48:155–181
Collander R (1951) Acta Chem Scand 5:774–780
Csik G, Balog E, Voszka I, et al (1998) J Photochem Photobiol B: Biol 44:216–224
Dixon DW, Steullet V (1998) J Inorg Biochem 69:25–32
Dougherty TJ, Gomer CJ, Henderson BW, et al (1998) J Natl Cancer I 90:889–905
Ehrenberg B, Anderson JL, Foote CS (1998) Photochem Photobiol 68:135–140
Eltayar N, Tsai RS, Testa B, et al (1991) J Pharm Sci 80:590–598
Engelmann FM, Losco P, Winnischofer H, et al (2002) J. Porphyrins Phthalocyanines 6:33–42
Engelmann FM, Rocha SVO, Araki K, et al (2007) Int J Pharm 329:12–18
Gabrielli D, Belisle E, Severino D, et al (2004) Photochem Photobiol 79:227–232
Henderson BW, Dougherty TJ (1992) Photochem Photobiol 55:145–157
Hidalgo AA, Tabak M, Oliveira ON (2005) Chem Phys Lipids 134:97–108

Junqueira HC, Severino D, Dias LG, et al (2002) Phys Chem Chem Phys 4:2320–2328
Kano K, Fukuda K, Wakami H, et al. (2000) J Am Chem Soc 122:7494–7502
Kepczynski M, Pandian RP, Smith KM, et al (2002) Photochem Photobiol 76:127–134
Kessel D, Luo Y (1998) J Photochem Photobiol B: Biol 42:89–95
Kessel D, Luo Y (1999) Cell Death and Differentiation 6:28–35
Khalili M, Grossweiner LI (1997) J Photochem Photobiol B: Biol 37:236–244
Kramer-Marek G, Serpa C, Szurko A (2006) J Photochem Photobiol B:Biol 84:1–14
Lambrechts SAG, Aalders MCG, Langeveld-Klerks DH (2004) Photochem Photobiol 79:297–302
Lambrechts SAG, Aalders MCG, Van Marle J (2005) Antimicrob Agents Chemother 49:2026–2034
Lavi A, Weitman H, Holmes RT, et al (2002) Biophys J 82:2101–2110
Lawrence DS, Gibson SL, Nguyen ML, et al (1995) Photochem Photobiol 61:90–98
Lemasters JJ (1999). Am J Physiol-Gastroint Liver Physiol 276:G1–G6
Lissi EA, Encinas MV, Lemp E, et al (1993) Chem Rev 93:699–723
Meng GG, James BR, Skov KA, et al (1994). Canadian J Chemistry-Revue Canadienne De Chimie 72:2447–2457
Merchat M, Spikes JD, Bertoloni G, et al (1996) J Photochem Photobiol B: Biol 35:149–157
Morgan J, Oseroff AR (2001) Advanced Drug Delivery Reviews 49:71–86
Netto LE, Kowaltowski AJ, Castilho RF, et al (2002) Methods Enzymol 260–270
Ochsner M (1997) J. Photochem Photobiol B: Biol 39:1–18
Parkash J, Robblee JH, Agnew J, et al (1998) Biophys J 74: 2089–2099
Reddi E, Ceccon M, Valduga G, et al (2002) Photochem Photobiol 75:462–470
Redmond RW, Gamlin JN (1999) Photochem Photobiol 70:391–475
Ricchelli F, Franchi L, Miotto G (2005) Int J Biochem 37:306–319
Rouser G, Fleische S, Yamamoto A (1970) Lipids 5:494
Schneckenburger H, Gschwend MH, Sailer R, Ruck A, and Strauss WSL (1995) J Photochem Photobiol B: Biol 27:251–255
Seiler P (1974) Eur J Med Chem 9:473–479
Severino D, Junqueira HC, Gabrielli DS, et al (2003) Photochem Photobiol 77:459–468
Silva EMP, Giuntini F, Faustino MAF, et al (2005) Bioorg Med Chem Lett 15:3333–3337
Smijs TGM, Schuitmaker HJ (2003) Photochem Photobiol 77:556–560
Spesia MB, Lazzeri D, Pascual L, et al (2005) FEMS Immunol Med Microbiol 44:289–295
Strauss WSL, Gschwend MH, Sailer R, et al (1995) J Photochem Photobiol B: Biol 28:155–161
Stromhaug PE, Berg TO, Berg K, et al (1997) Biochem J 321:217–225
Woodburn KW, Stylli S, Hill JS, et al (1992) Br J Cancer 65:321–328
Villanueva A, Jori G (1993) Cancer Lett 73:59–64
Voszka I, Galantai R, Maillard P, et al (1999) J Photochem Photobiol B: Biol 52:92–98
Zeitouni NC, Oseroff AR, Shieh S (2003) Mol Immunol 39:1133–1136